High-Performance Phototransistors Based on Single-Crystalline n-Channel Organic Nanowires and Photogenerated Charge-Carrier Behaviors

Hojeong Yu, Zhenan Bao, and Joon Hak Oh**

The photoelectronic characteristics of single-crystalline nanowire organic phototransistors (NW-OPTs) are studied using a high-performance n-channel organic semiconductor, *N*,*N*′-bis(2-phenylethyl)-perylene-3,4:9,10-tetracarboxylic diimide (BPE-PTCDI), as the photoactive layer. The optoelectronic performances of the NW-OPTs are analyzed by way of their current–voltage (*I*–*V*) characteristics on irradiation at different wavelengths, and comparison with corresponding thin-film organic phototransistors (OPTs). Significant enhancement in the charge-carrier mobility of NW-OPTs is observed upon light irradiation as compared with when performed in the dark. A mobility enhancement is observed when the incident optical power density increases and the wavelength of the light source matches the light-absorption range of the photoactive material. The photoswitching ratio is strongly dependent upon the incident optical power density, whereas the photoresponsivity is more dependent on matching the light-source wavelength with the maximum absorption range of the photoactive material. BPE-PTCDI NW-OPTs exhibit much higher external quantum efficiency (EQE) values (≈7900 times larger) than thin-film OPTs, with a maximum EQE of 263 000%. This is attributed to the intrinsically defect-free single-crystalline nature of the BPE-PTCDI NWs. In addition, an approach is devised to analyze the charge-transport behaviors using charge accumulation/release rates from deep traps under on/off switching of external light sources.

1. Introduction

Phototransistors are transistors in which the incident light intensity can modulate the charge-carrier density in the channel.[1] Compared with photodiodes that have two electrodes, phototransistors enable easier control of light-detection sensitivity without problems such as the noise increment associated with conventional avalanche photodiodes due to the presence of an additional (i.e., third) electrode for amplifying the electrical signals induced by the incoming photons.[2] While inorganic phototransistors have been extensively exploited and are currently commercially available, organic phototransistors (OPTs) are less studied.[3–10] OPTs have many intrinsic advantages over their inorganic counterparts, such as the chemical tunability of optoelectronic properties by molecular design and high potential in low-cost, light-weight, flexible applications.

Single-crystalline nano-/microwires (NWs/MWs) based on organic semiconductors have attracted great interest recently as they are promising building blocks for various electronic and optoelectronic applications such as light-emitting diodes (LEDs),[11] field-effect transistors (FETs),[12,13] photoswitches,[9,14] sensors,[15] solar cells,[16] nanoscale lasers,[17] optical waveguides,[18] and memory devices.[19] In particular, OPTs based on single-crystalline NWs/MWs may yield higher light sensitivity than their bulk counterparts due to the lack of grain boundaries that act as an energetic barrier for charge transport.[20] In addition, their one-dimensional, intrinsically defect-free and highly ordered nature will allow a deeper understanding of the fundamental mechanisms of charge generation and transport in OPTs, while enabling a bottom-up fabrication of optoelectronic nanodevices. Although a number of organic semiconducting materials, such as small molecules, polymers, and their mixtures, have been used for bulk thin-film OPTs,[4,6–8,21–24] single-crystalline NWs/MWs have been far less employed for OPTs.[3,9,25] Furthermore, most reports on single-crystalline OPTs have utilized p-channel materials. The development of OPTs based on n-channel single-crystalline organic semiconducting NWs/MWs is highly desirable for the bottom-up fabrication of complementary metal oxide semiconductor (CMOS)-like photoelectronic circuits, which provides various advantages such as high operational stability, easy control of photoswitching voltages, high photosensitivity and responsivity.

H. Yu, Prof. J. H. Oh
School of Nano-Bioscience and Chemical Engineering
KIER-UNIST Advanced Center for Energy
Low Dimensional Carbon Materials Center
Ulsan National Institute of
Science and Technology (UNIST)
Ulsan 689-798, South Korea
E-mail: joonhoh@unist.ac.kr
Prof. Z. Bao
Department of Chemical Engineering
Stanford University
381 North South Mall, Stanford, CA 94305, USA
E-mail: zbao@stanford.edu

DOI: 10.1002/adfm.201201848

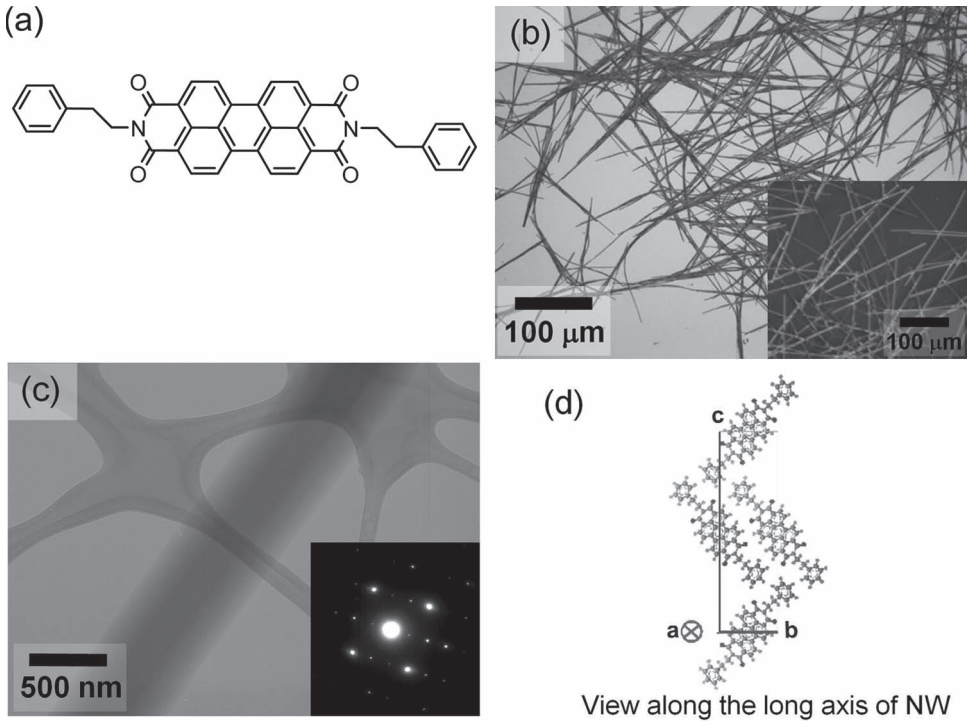

Figure 1. a) The chemical structure of BPE-PTCDI. b) A bright-field optical microscopy image of the BPE-PTCDI NWs. The inset shows a dark-field optical image of the NWs. c) A TEM image of a BPE-PTCDI single NW. The inset shows a selected area electron diffraction (SAED) pattern. d) The molecular packing viewed along the long axis of a single NW with the unit lattice constants of $a = 8.7$ Å, $b = 4.7$ Å, $\gamma = 79°$.

Herein, we report photoelectronic properties of organic single-crystalline n-channel nanowire OPTs (NW-OPTs) fabricated using an air-stable, high-performance n-channel organic semiconductor, *N,N′*-bis(2-phenylethyl)-perylene-3,4:9,10-tetracarboxylic diimide (BPE-PTCDI) (**Figure 1**a),[13] as the photoactive layer. The photoelectronic characteristics of the single-crystalline NW-OPTs, such as the photoresponsivity, the photoswitching ratio, and the photoconductive gain, were analyzed from the *I–V* characteristics coupled with light irradiation and compared with those of vacuum-deposited thin-film devices. The external quantum efficiencies (EQEs) were also investigated for the NW-OPTs and thin-film OPTs. In addition, we calculated the charge accumulation and release rates from deep traps, and investigated the effects of incident light intensity on their photoelectronic properties.

2. Results and Discussion

2.1. Fabrication and Characterizations of BPE-PTCDI NWs/MWs

BPE-PTCDI NWs were fabricated with the nonsolvent nucleation method or the solvent-exchange method, as reported previously.[13,14,26] BPE-PTCDI molecules are sparingly soluble in a common organic solvent such as *o*-dichlorobenzene at room temperature, whereas they become soluble at an elevated temperature (typically ≥ 150 °C). Upon cooling, BPE-PTCDI molecules recrystallize rapidly due to the reduced solubility. The strong cofacial π–π interactions lead to the formation of one-dimensional supramolecular assemblies. Adding a nonsolvent (e.g., methyl alcohol) into the hot, homogeneous solution results in the immediate formation of nucleating sites and thus reducing the dimension of the resulting wires. This is similar to the general principle used in free-radical polymerization, in which the molecular weights of the polymers are reduced by adding more radical initiators, which subsequently increases the number of reactive initiating species for polymerization.[27]

The size of BPE-PTCDI wires could be readily tuned by controlling the cooling speed and the solvent mixing ratio, ranging from several tens of nanometers to several micrometers in diameter and several tens of micrometers to several millimeters in length. The typical optical microscopy images of the BPE-PTCDI NWs fabricated by using 11.8 vol% of methyl alcohol are illustrated in Figure 1b. Its inset exhibits a dark-field image of the NWs, revealing their highly crystalline nature. The molecular packing and crystal structure of the BPE-PTCDI NWs were characterized using transmission electron microscopy (TEM). A typical TEM image and the selected area electron diffraction (SAED) pattern (inset) of a BPE-PTCDI NW are shown in Figure 1c. A number of diffraction patterns obtained at different locations of the same wire exhibited the same crystal-phase geometry, indicating the single-crystalline nature of the BPE-PTCDI NWs.[13] The diffraction patterns taken on a single NW correspond to a single-crystalline phase with unit lattice constants of $a = 8.7$ Å, $b = 4.7$ Å, $\gamma = 79°$, which is similar to the previously reported structure for these NWs and corresponds to the (010) plane of the bulk crystal (Figure 1d).[28] The growth direction of the wire is the *a*-axis with the shortest π-planar distance of 3.4 Å, indicating that most-efficient charge-transport pathway occurs along the long axis of the nanowire.[14,29,30]

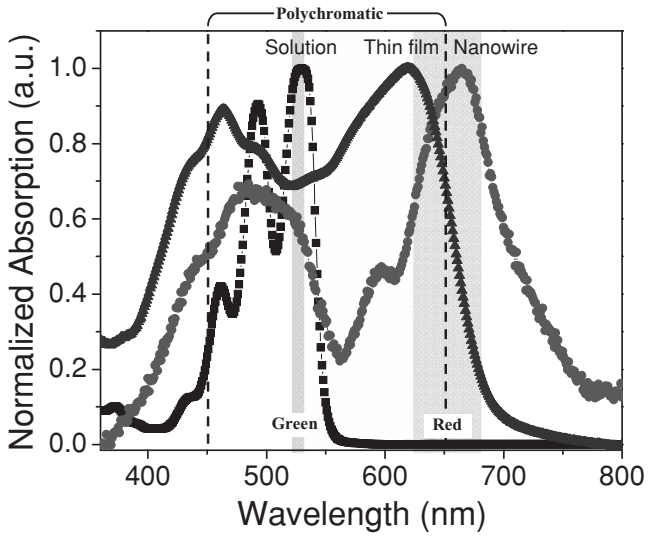

Figure 2. UV–vis spectra of BPE-PTCDI solution in *o*-dichlorobenzene at 150 °C, vacuum-deposited thin film, and a NW network film. The wavelength regions of different light sources (red, green, and polychromatic light) are included for a guideline. The rectangles around 532 nm and 635–680 nm indicate the wavelengths of the green and red light sources, respectively. The dotted rectangle represents the wavelength region of the polychromatic light source.

UV–vis spectra of BPE-PTCDI solution in *o*-dichlorobenzene at 150 °C, vacuum-deposited thin film, and a NW network film are all illustrated in **Figure 2**. The corresponding wavelength region of each light source (vide infra) is also depicted as a guideline. In solution, the absorption bands at 533, 494, 462, and 433 nm correspond to the 0–0, 0–1, 0–2, and 0–3 transitions of the vibronic structure of individual BPE-PTCDI molecules, respectively. The maximum absorption wavelengths (λ_{max}) of the thin film and NWs were observed at 620 and 665 nm, respectively. The red-shifted absorption bands indicated that BPE-PTCDI molecules form J-aggregates in the self-assembled structures, similar to other PTCDI derivatives.[31,32] The highest occupied molecular orbital (HOMO), the lowest unoccupied molecular orbital (LUMO) energy levels, and the band gaps of BPE-PTCDI in the solution state,[33,34] the thin films, and the NWs are all presented in **Table 1**. Due to the enhanced electronic coupling between molecules in crystalline solids, the LUMO levels became lower as the levels of structural perfection increased.[35] Judging from the long-wavelength absorption edge in the UV–vis spectra, the optical bandgaps of BPE-PTCDI in solution, thin film, and NWs were estimated to be 2.25, 1.81, 1.65 eV, respectively.

2.2. Optoelectronic Performance of NW-OPTs and Thin-Film OPTs

To investigate the effects of incident light on the charge-carrier behaviors of NW-OPTs, we prepared BPE-PTCDI NW-OPTs containing an individual BPE-PTCDI NW as the active material on *n*-octadecyltrimethoxysilane (OTS)-treated SiO_2/Si and bare SiO_2/Si substrates in either bottom-contact or top-contact configuration (see Experimental Section for more details). The corresponding device structures are depicted in **Figure 3**. The active channel dimensions were estimated from the width (W) and length (L) of the NW crossing the source and drain electrodes. The photoelectronic properties were investigated using different light sources available in our laboratory (i.e., green (λ = 532 nm, P_{max} = 113 mW cm^{-2}), red (λ = 635–680 nm, P_{max} = 14 mW cm^{-2}), and polychromatic light (λ = 450–650 nm, P_{max} = 36 mW cm^{-2}).

Table 1 A summary of the HOMO and LUMO levels of BPE-PTCDI in the solution state, the vacuum-deposited thin film, and the NW form.

Sample	HOMO [eV]	LUMO [eV]	E_g [eV]
Solution[a)]	−6.10	−4.10	2.00 (2.25)[d)]
Thin Film[b)]	−6.07[c)]	−4.26	1.81[d)]
Nanowire	−6.04[c)]	−4.39	1.65[d)]

[a)]Literature values[33,34] measured by cyclic voltammetry; [b)]The 45 nm thin film made by evaporation under high vacuum (≈10^{-6} Torr) at a deposition temperature of 125 °C; [c)]Workfunction measured in ambient air by ultraviolet photoelectron spectroscopy (UPS); [d)]The bandgap, the long wavelength absorption edge on the UV–vis spectra.

In the bottom-contact configuration, twelve randomly chosen BPE-PTCDI NW-OPTs exhibited an average electron mobility of 0.62 ± 0.41 cm^2 V^{-1} s^{-1} and 0.035 ± 0.012 cm^2 V^{-1} s^{-1} on OTS-treated SiO_2/Si and bare SiO_2/Si substrates, respectively, under dark conditions. The large difference in the charge-carrier mobility is hypothesized to originate from the difference in the electron-trap density and the contact quality at the NW/insulator and NW/electrode interfaces.[13,36]

A significant mobility enhancement was observed when the BPE-PTCDI NW-OPTs were exposed to an external light source. **Figure 4**a exhibits the normalized mobility increment of bottom-contact NW-OPTs when compared to that in dark conditions. The charge-carrier mobility of the NW-OPTs in the dark increased up to 13 times upon exposure to red light (P_{max} = 14 mW cm^{-2}), whereas green monochromatic light irradiation (P_{max} = 113 mW cm^{-2}) yielded a mobility >20 times greater. In particular, red light (P_{max} = 14 mW cm^{-2}) illumination exhibited a larger increment in the mobility compared to polychromatic light (P_{max} = 36 mW cm^{-2}), despite the smaller optical power density. This is attributed to the fact that the

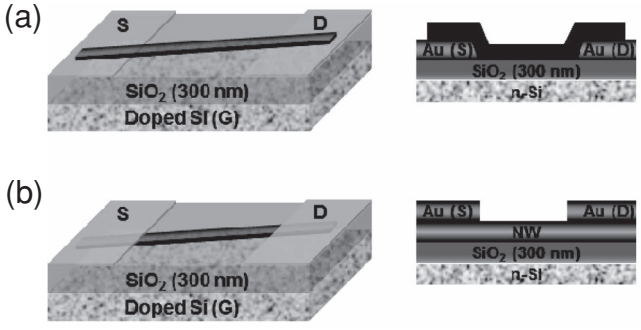

Figure 3. Device structures of BPE-PTCDI single NW-OPTs: a) bottom-contact configuration, and b) top-contact configuration.

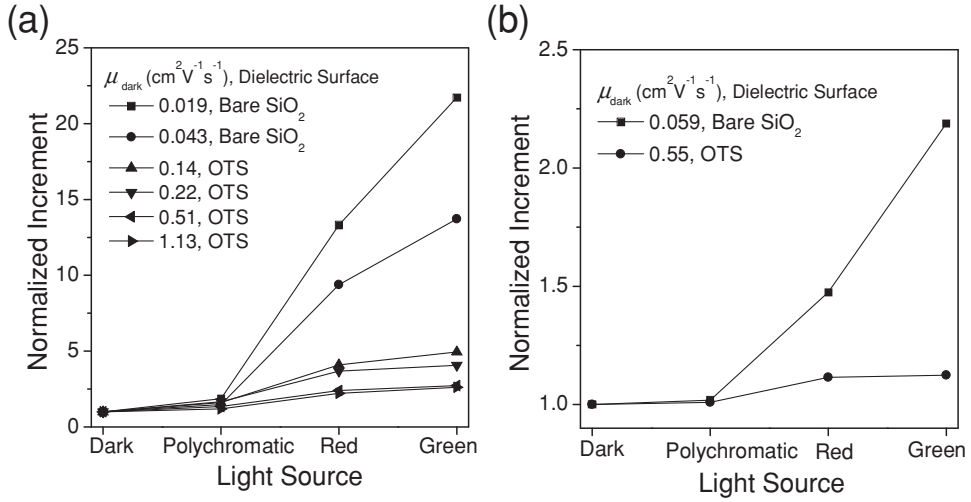

Figure 4. Mobility enhancement upon irradiation of different light sources for: a) bottom-contact NW-OPTs and b) top-contact NW-OPTs prepared on OTS-treated SiO_2/Si and bare SiO_2/Si substrates.

absorption of BPE-PTCDI NW is relatively stronger in the red light region (Figure 2). Intriguingly, the relative increment in mobility became larger for devices with a lower mobility under dark conditions. Presumably, the incoming photons fill and eliminate a larger number of traps in a device with a lower mobility.

As a comparison, NW-OPTs were additionally prepared in top-contact configuration by thermally evaporating gold source and drain electrodes on top of individual BPE-PTCDI NWs. In the top-contact NW-OPTs, the average mobilities of five randomly chosen devices under dark condition were 0.53 ± 0.24 $cm^2\ V^{-1}\ s^{-1}$ and 0.058 ± 0.036 $cm^2\ V^{-1}s^{-1}$ on OTS-treated SiO_2/Si and bare SiO_2/Si substrates, respectively. Figure 4b shows the representative mobility enhancement of the top-contact NW-OPTs. The lower mobility device showed an increased carrier mobility up to a value >2 times higher upon exposure to green light. The increment in mobility was relatively smaller than that of bottom-contact devices. Blocking of incoming light by gold electrodes in the contact area might reduce the photocurrent enhancement, indicating that light irradiation significantly affects the charge-injection behavior in OPT devices.

Figure 5a,b show transfer characteristics of bottom-contact BPE-PTCDI NW-OPTs with dark-condition mobilities (μ_{dark}) of 1.13 and 0.216 $cm^2\ V^{-1}\ s^{-1}$, respectively, upon irradiation with different light at a drain voltage (V_D) bias of 100 V. Under light irradiation, the off-current of the NW-OPTs significantly increased due to the photocurrent. In addition, the threshold voltage (V_T) shifted negatively, implying the easier turn-on of

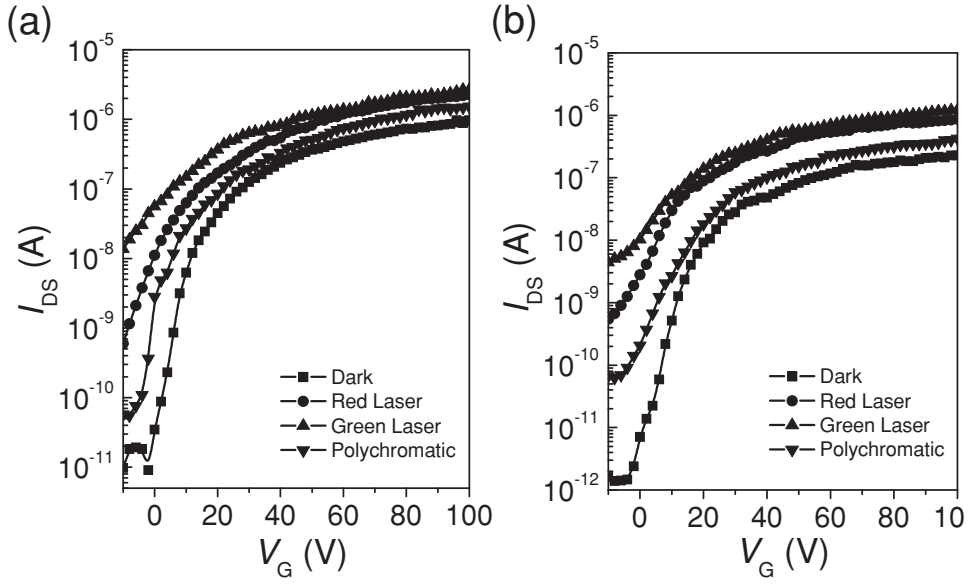

Figure 5. I_{DS}–V_G characteristics in the dark or under different light irradiations, recorded with V_D = 100 V for the bottom-contact NW-OPTs with a dark-condition mobility (μ_{dark}) of: a) 1.13 $cm^2\ V^{-1}\ s^{-1}$ at W/L = 0.0675; and b) 0.216 $cm^2\ V^{-1}\ s^{-1}$ at W/L = 0.0915.

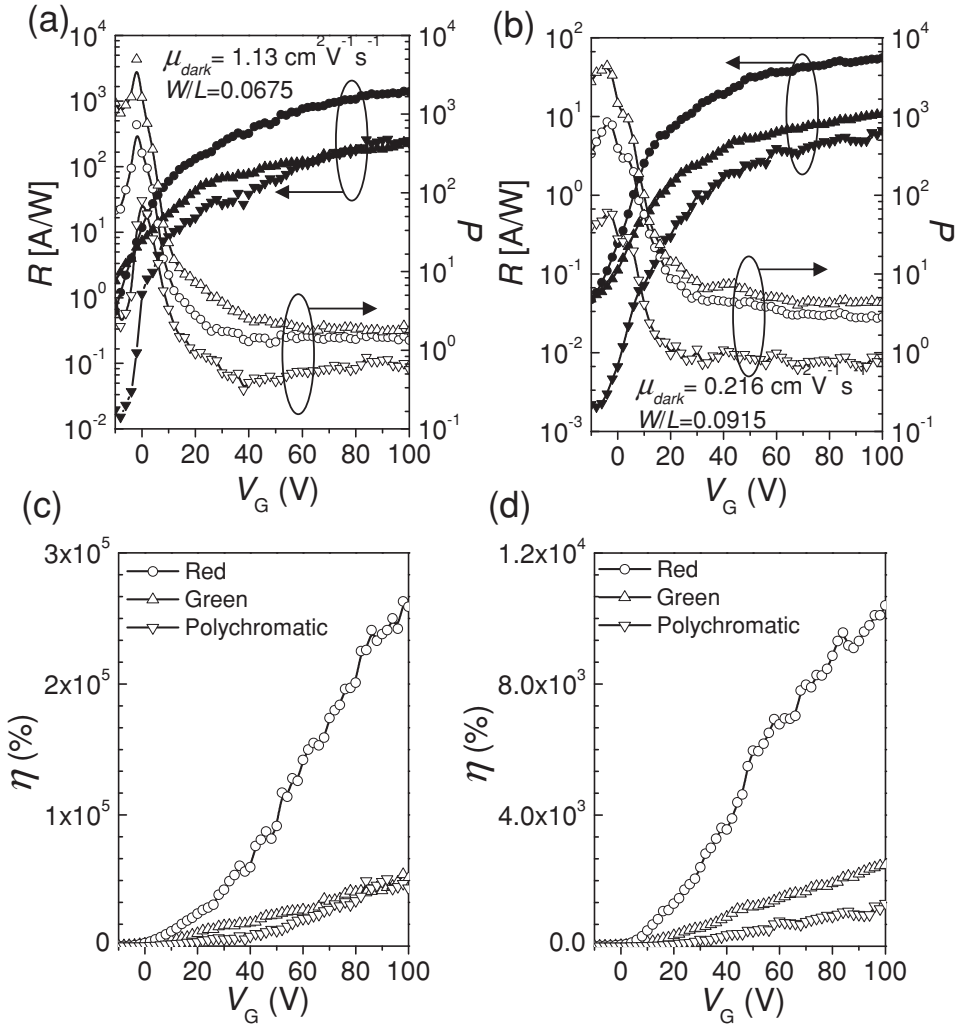

Figure 6. Responsivity (R), photocurrent/dark-current ratio (P), and external quantum efficiency (EQE) (η) of single NW-OPTs as a function of V_G for: a,c) NW-OPTs with μ_{dark} = 1.13 cm^2 V^{-1} s^{-1} or b,d) μ_{dark} = 0.216 cm^2 V^{-1} s^{-1}. The circle, triangle, and inverted-triangle symbols represent the irradiation of red, green, and polychromatic light, respectively.

the device. This can be attributed to the elimination of trap sites by the photogenerated charge carriers.[8,37,38] Green light irradiation yielded the largest enhancement in the drain current (I_{DS}). However, it is noteworthy that red light illumination exhibited similarly high I_{DS}, despite the smaller optical power density than green light, due to the larger absorption of incoming photons.

Light responsivity (R) and photocurrent/dark-current ratio (P) are important parameters for investigating photosensitivity for OPTs and those values can be determined from transfer characteristics coupled with light irradiation. The R and P values are typically defined by the following equations:[3]

$$R = \frac{I_{ph}}{P_{inc}} = \frac{I_{light} - I_{dark}}{P_{inc}} \quad (1)$$

$$P = \frac{(I_{light} - I_{dark})}{I_{dark}} \quad (2)$$

where I_{ph} is the photocurrent, P_{inc} the incident illumination power on the channel of the device, I_{light} the drain current under illumination, and I_{dark} the drain current in the dark. The R and P values were plotted as a function of V_G for the NW-OPTs with a high mobility of 1.13 cm^2 V^{-1} s^{-1} and a low mobility of 0.216 cm^2 V^{-1} s^{-1} (**Figure 6**a,b, respectively).

The maximum P was observed in the off-state under green light irradiation, while the maximum R was obtained in the on-state (V_G = 100 V) under red light irradiation. This indicates that P is strongly dependent upon the incident optical power density, whereas R is more related to the matching between the light-source wavelength and the absorption range of the photoactive material (see UV–vis absorption spectra in Figure 2). The NW-OPT device with a high mobility (1.13 cm^2 V^{-1} s^{-1}) showed a maximum R of 1.40×10^3 A W^{-1} and P of 4.96×10^3 under red and green light irradiation, respectively (Figure 6a). The R value of the BPE-PTCDI single NW-OPT is higher than that (1.18×10^2 A W^{-1}) for single-fiber OPTs based on other PTCDI derivatives with alkyl side chains, while those multifiber-based OPTs

exhibited a maximum R of 4.08×10^5 A W^{-1}.[39] On the other hand, the NW-OPT device with a low mobility (0.216 cm^2 V^{-1} s^{-1}) yielded a maximum R of 5.56×10^1 A W^{-1} and P of 4.40×10^3 under red and green light irradiation, respectively (Figure 6b). This indicates that R is strongly dependent on μ_{dark}, while P is not much dependent on the μ_{dark}.

In addition, the external quantum efficiency (EQE) (η) of OPTs can be defined as the ratio of the number of photogenerated carriers that practically enhances the drain current to the number of photons incident onto the OPT channel area, using the following equation:[6]

$$\eta = \frac{\left(I_{light} - I_{dark}\right) hc}{e P_{inc} A \lambda_{peak}} \quad (3)$$

where h is the Planck constant, c the speed of light, e the fundamental unit of charge, A the area of the transistor channel, and λ_{peak} the peak wavelength of the incident light. Figure 6c,d depict EQEs for the NW-OPTs with μ_{dark} values of 1.13 cm^2 V^{-1} s^{-1} and 0.216 cm^2 V^{-1} s^{-1}, respectively (V_D = 100 V). Surprisingly, the NW-OPT with the high μ_{dark} of 1.13 cm^2 V^{-1} s^{-1} exhibited a very high EQE value up to 263 000% at V_G = 100 V under red light irradiation, while the NW-OPT with the lower mobility (0.216 cm^2 V^{-1} s^{-1}) showed an EQE of 10 400% at the same condition. These EQE values are much higher than those of other high-performance inorganic photodiodes and organic phototransistors such as n$^+$p Si photodiodes (>3000%)[40] and vertical polymer phototransistors (360%).[41] As the EQE values are higher than 100%, this indicates that BPE-PTCDI NW-OPTs exhibit the photomultiplication (PM) phenomenon,[1] making them a highly promising alternative to conventional thin-film-type avalanche diodes.

In principle, impact ionization is virtually impossible in disordered organic materials owing to the strong carrier localization; thereby, EQEs higher than 100% cannot be easily obtained in amorphous or polycrystalline organic domains.[42] However, Hiramoto and coworkers observed photomultiplication in organic diodes, which was attributed to the photoinduced electron injection occurring at the semiconductor/metal interface (i.e., the principle of a field-modulated tunneling barrier).[43–45] In addition, Reynaert and coworkers found that energetic disorder can strongly facilitate photomultiplication even in a random-hopping system in which impact ionization would be impossible at a realistic electric-field strength.[46] In BPE-PTCDI NW-OPTs, photoexcitation may cause a high density of accumulated holes at the semiconductor/electrode interface, and then tunneling electrons eventually result in photocurrent multiplication, similarly to organic photodiodes.[43] In addition, the incident light possibly causes a fast supply of charge carriers to the semiconductor/electrode and semiconductor/dielectric interface owing to the single-crystalline nature of the NW, thereby effectively filling traps and allowing a higher mobility and a higher current.

As a comparison, the photoelectrical behaviors of BPE-PTCDI thin-film OPTs were also investigated. The device structure and the transfer characteristics are shown in **Figure 7**a,b, respectively. The thin-film OPTs exhibited a mobility of 0.018 ± 0.015 cm^2 V^{-1} s^{-1} under dark conditions and 0.039 ± 0.025 cm^2 V^{-1} s^{-1} under irradiation of polychromatic light (36 mW cm^{-2}). The R and P values of the BPE-PTCDI thin-film OPTs are illustrated in Figure 7c. The thin-film OPT device showed a maximum R of 3.38×10^{-2} A W^{-1} and P of 1.85×10^3. EQE measurements under irradiation of polychromatic light revealed that the maximum EQE of the thin-film OPTs was only 6.5% at V_G = 52 V (Figure 7d), which is far less than those of NW-OPTs (≈1300–51 200% for NW-OPTs under the same light source). The downshift of V_G showing the maximum EQE is mainly related with the saturation of the drain current at a lower V_G for thin-film OPTs compared with NW-OPTs. The much higher EQE values of the NW-OPTs may be due to the defect-free, single-crystalline nature of BPE-PTCDI NW that allows a longer exciton diffusion length as well as a lower energetic barrier for charge-carrier transport.[12,13,47] The fewer traps in single crystals possibly cause a quick supply of charge carriers,[45] and thus the same bias voltage can multiply photoinduced charge carriers up to many orders of magnitude. In contrast, a large number of grain boundaries in thin films act as trap sites to fill, leading to a lower EQE. In addition, the relatively smaller bandgap of BPE-PTCDI NW (1.65 eV) than in the thin-film counterpart (1.81 eV) may cause a larger amount of absorption of incident photons, thereby yielding a greater amount of photogenerated charge carriers and a higher gate-field shielding effect.[41]

2.3. Photoswitching Characteristics of NW-OPTs and Thin-Film OPTs

To further substantiate the potential of BPE-PTCDI NWs in optoelectronic applications, their photoresponses upon on-and-off switching of light were investigated. The bottom-contact NW-OPTs exhibited a highly reproducible, high photosensitivity. Interestingly, a specific trend of charge accumulation and release was observed at the initial stage of turn-on and turn-off of light (see Section 2.4. for quantitative evaluations). The off-state (V_G = 0 V, V_D = 100 V) and the on-state (V_G = 100 V, V_D = 100 V) photocurrents of the NW-OPTs were recorded under polychromatic light (**Figure 8**a,b, respectively). The off-state measurement revealed how electron carriers respond under light (i.e., on-and-off conditions) without the aid of an external gate field (Figure 8a). The generation of additional excitons by sufficiently intense light produced nanoampère-scale photocurrents.

The photoswitching characteristics of BPE-PTCDI thin-film OPTs were also investigated in the off-state (Figure 8c) and the on-state (Figure 8d). Compared with the NW-OPTs, the thin-film OPTs exhibited a much lower photosensitivity and photoconductive gain. Interestingly, the photoresponse of the thin-film OPTs in the on-state was significantly different compared with that of the NW-OPTs (see Figure 8b and 8d). The NW-OPTs showed substantially enhanced photocurrent gain on light exposure, whereas the thin-film OPTs exhibited only a slight increase in current upon light irradiation with a gradually decreasing drain-current baseline. This indicates that the thin-film OPTs are more vulnerable to the high voltage bias in the on-state.

The on-state current density normalized by the active area revealed that NW-OPTs yielded a current density of 10^{-3} A mm^{-2},

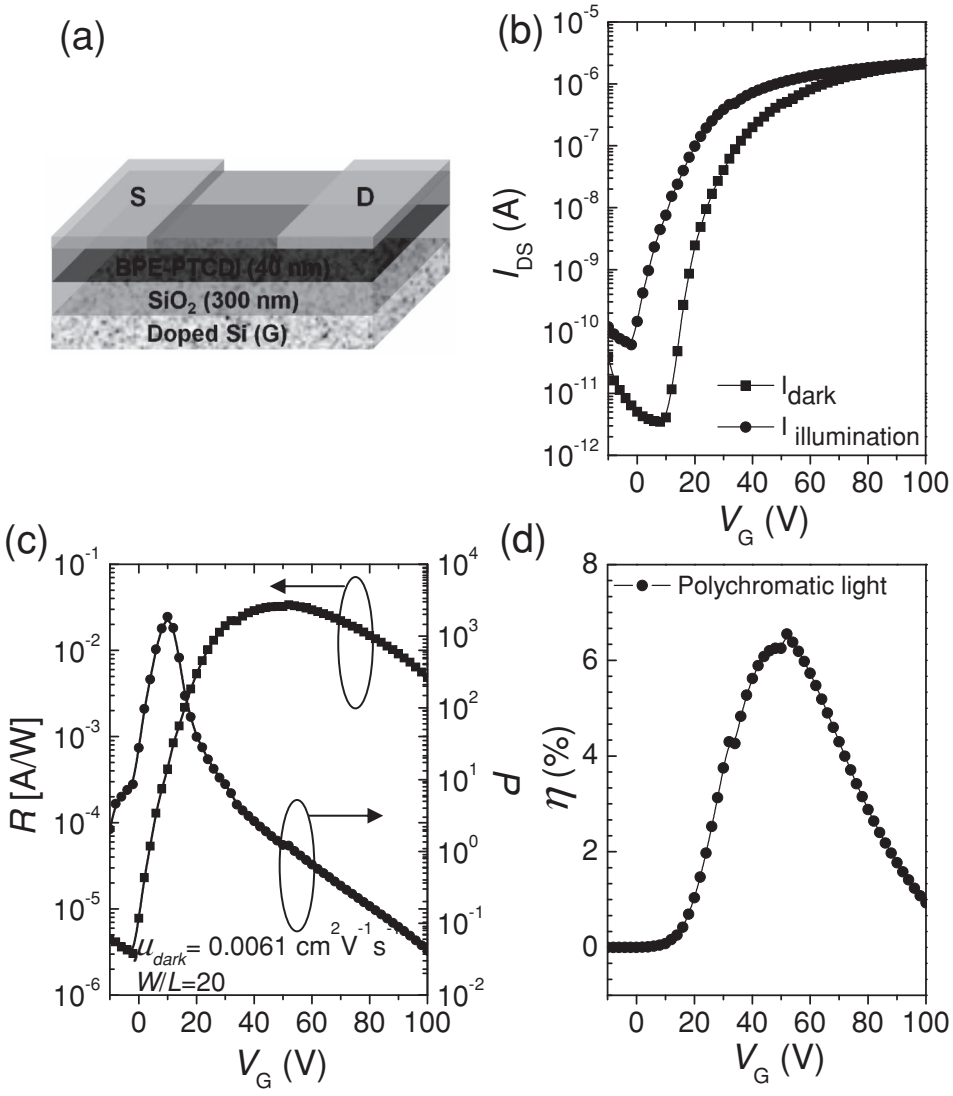

Figure 7. a) Device structure of BPE-PTCDI thin-film OPT. b) Transfer characteristics based on a thin-film OPT in the dark and under polychromatic light irradiation with an optical power density of 36 mW cm^{-2}. c) Responsivity (R) and photocurrent/dark-current ratio (P) of thin-film OPTs. d) EQE (η) of thin-film OPTs as a function of V_G.

which is ≈10^4 times higher than the thin-film OPTs. These results indicate that the single-crystalline NW-OPTs showed significantly higher light sensitivity and photoconductivity than their thin-film counterparts. As described above, the normalized EQEs of the NW-OPTs were amplified to a substantially higher gain (EQE ≈7900-fold larger) compared to the thin-film OPTs under polychromatic light, indicating that organic single-crystalline NWs can be utilized for optoelectronic device miniaturization.

2.4. Charge Accumulation/Release Rates

The interesting phenomena of charge accumulation and release have frequently been observed at the initial stage of turn-on and turn-off of light for previously reported OPTs.[9,48,49] To the best of our knowledge, however, these behaviors have largely been ignored and have not been studied systematically. Here, we investigated charge accumulation and release rates from deep traps by modifying the conventional transistor equation in the saturation-regime ($V_D \geq (V_G - V_T)$).[27] In a device upon operation in the saturation regime, the threshold voltage (V_T) can be expressed as a function of illumination time (t) by the following equation:

$$V_T = V_G - \left[\frac{2 I_D(t) L}{\mu_{sat} C W}\right]^{1/2} \quad (4)$$

where C is the insulator capacitance per unit area, W the channel width, L the channel length, and μ_{sat} the saturation-regime mobility. According to Equation 4, the charge release rate from the deep traps is defined as follows:

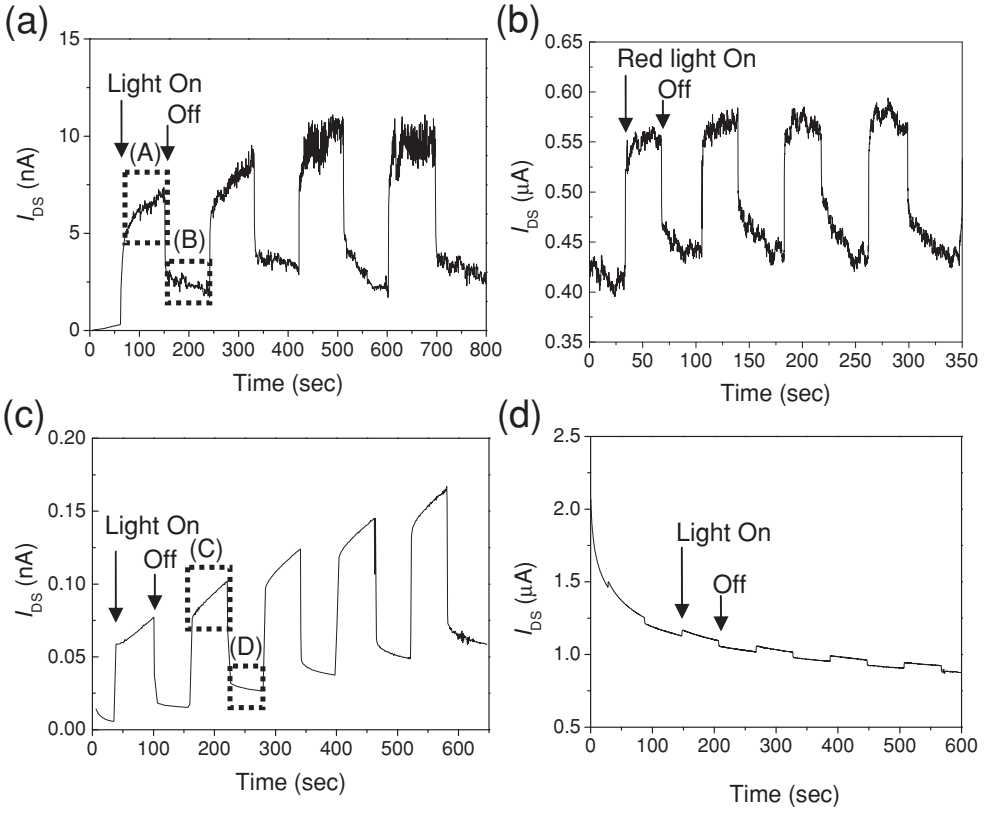

Figure 8. The on/off switching of BPE-PTCDI NW-OPTs upon: a) polychromatic light illumination with a power of 36 mW cm^{-2}; and b) red light illumination with a power of 14 mW cm^{-2}. c,d) Photoswitching behaviors of BPE-PTCDI thin-film OPTs under on/off switching of polychromatic light. The devices were measured at a,c) V_G = 0 V and V_D = 100 V and b,d) at V_G = 100 V and V_D = 100 V. The dotted rectangular regions of (A), (B), (C) and (D) were used for the calculation of charge-carrier accumulation and release rates.

$$\text{rate} = \frac{dQ}{dt} = C\frac{dV_T(t)}{dt} = -\left[\frac{2LC}{\mu_{sat}W}\right]^{1/2}\frac{d\left(I_D(t)\right)^{1/2}}{dt} \quad (5)$$

which indicates how the additional free-charge-carrier density varies quantitatively upon exposure to light. The upward trend of the photocurrent upon light irradiation and the downward trend under turning off the light condition are related to charge accumulation and release, respectively.

The average accumulation and release rates of charge carriers were calculated using Equation 5 and applying a least-squares linear fit. The charge accumulation rate in the BPE-PTCDI NW-OPT under polychromatic light was found to be 2.76 × 10^9 cm^{-2} s^{-1} (Region A in Figure 8a). After turning off the light, the accumulated charges were released at a rate of 1.17 × 10^9 cm^{-2} s^{-1} (Region B in Figure 8a). On the contrary, in the case of BPE-PTCDI thin-film OPTs, charge carriers were accumulated at a rate of 5.67 × 10^7 cm^{-2} s^{-1} (Region C in Figure 8c) and released at a rate of 1.62 × 10^7 cm^{-2} s^{-1} (Region D in Figure 8c). It turns out that single-crystalline BPE-PTCDI NWs exhibit faster charge accumulation/release compared with the vacuum-deposited thin films.

The effects of light source on the charge accumulation/release rates were also investigated. **Figure 9** exhibits the drain-current response of BPE-PTCDI NW-OPTs for on-and-off switching of polychromatic, green, and red light illuminations (Figure 9a, 9b, and 9c, respectively) in the transistor on-state (V_G = 100 V, V_D = 100 V). Figure 9d,e illustrate calculations of the charge accumulation/release rates for each photoelectrical response. The highest values in the charge accumulation rate (3.78 × 10^{12} cm^{-2} s^{-1}) and release rate (3.92 × 10^{12} cm^{-2} s^{-1}) were observed from green light illumination, most likely due to its strongest light intensity. Similarly high values of the charge accumulation (1.39 × 10^{12} cm^{-2} s^{-1}) and release (2.60 × 10^{12} cm^{-2} s^{-1}) rates under red light illumination with a lower optical power density revealed that charge accumulation/release rates can also be enhanced by optimizing the wavelength of the incident light to the absorption band of the photoactive layer.

3. Conclusions

We have successfully fabricated high-performance n-channel NW-OPTs based on single-crystalline BPE-PTCDI NWs and have characterized the photoelectronic properties. Red monochromatic light yielded a significant mobility enhancement up to 13 times on NW-OPTs due to its stronger absorption, despite the smaller optical power density (P_{max} = 14 mW cm^{-2}) than polychromatic light (P_{max} = 36 mW cm^{-2}). The NW-OPT device

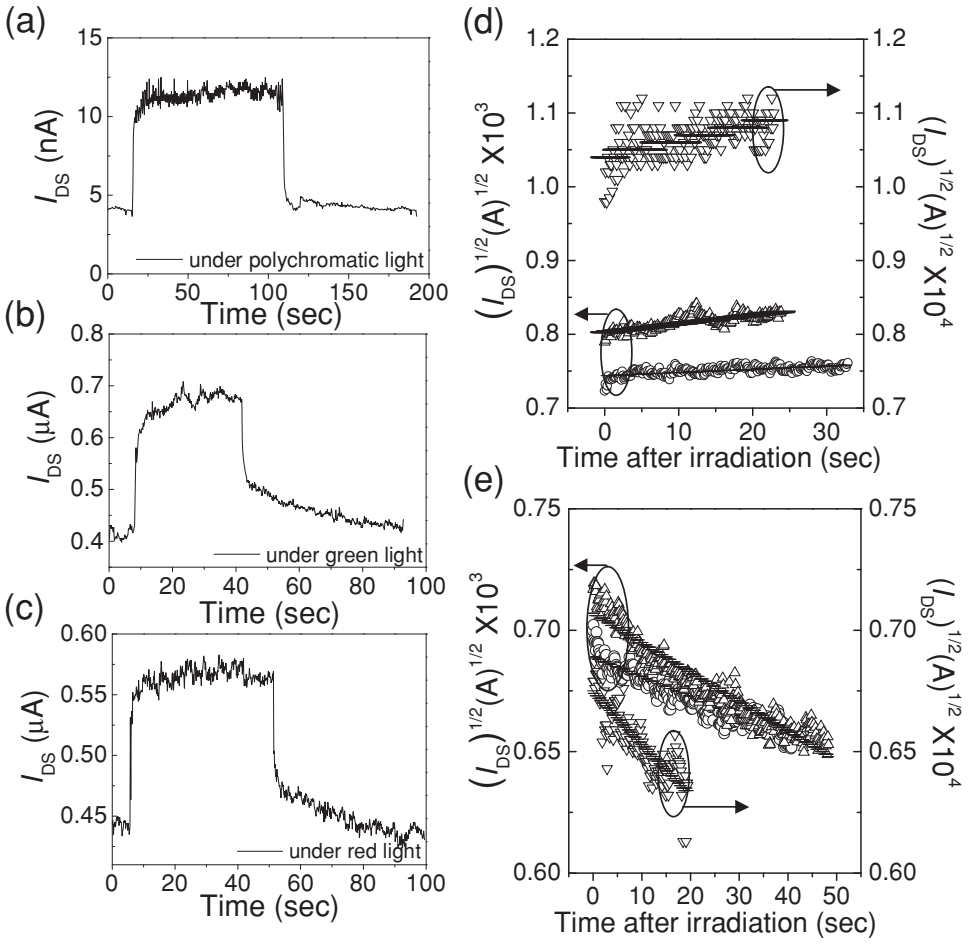

Figure 9. Switch-on and switch-off optical responses of bottom-contact NW-OPTs at V_D = 100 V and V_G = 100 V, as a function of time under a pulsed light illumination: a) polychromatic light, b) green light, and c) red light. d,e) Charge accumulation (d) and release rate (e) calculations using Equation 5 and applying a least-squares linear fit. The circle, triangle, and inverted-triangle symbols correspond to the red, green, and polychromatic light sources, respectively.

with a higher mobility (1.13 cm^2 V^{-1} s^{-1}) showed good photoresponse properties with a maximum light responsivity (R) of 1.4 × 10^3 A W^{-1} and a maximum photocurrent/dark-current ratio (P) of 4.96 × 10^3 under red and green light irradiation, respectively. We observed that P is strongly dependent upon the incident optical power density, whereas R is dependent on matching the light-source wavelength with the maximum absorption range of the photoactive material. Furthermore, we observed that BPE-PTCDI NW-OPTs exhibited an EQE value up to 263 000% at V_G = 100 V under red light exposure, most likely due to the photomultiplication phenomenon by the field-modulated tunneling effects and the intrinsic properties of BPE-PTCDI NW platform. In contrast, vacuum-deposited thin-film OPTs yielded only an EQE of 6.5% at V_G = 52 V under the polychromatic light. We found that the normalized EQEs of the NW-OPTs could be amplified to a substantially higher gain (EQE ≈7900-fold larger) compared with thin-film OPTs under polychromatic light.

Moreover, the single-crystalline NWs-OPTs exhibited faster charge accumulation/release rates than those of thin-film OPTs. The charge accumulation and release rates could also be enhanced by simply tuning the wavelength of the incident light to the absorption band. Our described approach to charge-accumulation/release-rate calculations could provide a fundamental understanding about charge-carrier-density variations under light irradiation, which subsequently enables in-depth study of OPTs. Hence, organic single-crystalline NW-OPTs are a highly promising alternative to conventional thin-film-type photodiodes, and can effectively pave the way for optoelectronic device miniaturization.

4. Experimental Section

Preparation of BPE-PTCDI NWs:[13] BPE-PTCDI (9 mg) was dissolved in refluxing *o*-dichlorobenzene (7.5 mL) in a round-bottom flask with stirring. In the nonsolvent nucleation method, methyl alcohol (1.5 mL) was added into the solution, which was then stirred for 30 s. This led to the immediate formation of nuclei for crystal growth. After several hours, BPE-PTCDI NWs were observed in the flask and the solution was then vacuum-filtered with a porous anodized aluminum oxide (AAO). During the filtration, the BPE-PTCDI NWs were washed with an excess amount of ethyl alcohol, and redispersed in a vial containing ethyl alcohol.

Fabrication and Characterization of NW-OPTs and Thin-Film OPTs: NW-OPTs were fabricated with a heavily n-doped Si wafers covered with a 300 nm-thick SiO_2 dielectric (C_i = 10 nF cm^{-2}). The bottom-contact devices were prepared by defining source-drain electrodes via conventional photolithography on top of SiO_2/Si wafers. The electrode-patterned wafers were treated with vaporized *n*-octadecyltrimethoxysilane (OTS). A few drops of OTS were loaded in a vial inside a vacuum desiccator. The desiccator was immediately evacuated under vacuum. The electrode-patterned wafers were treated to give a hydrophobic surface at 110 °C for 12 h. NW-OFTs were fabricated by drop-casting a BPE-PTCDI NW solution on the electrode-patterned substrate. For the top-contact device fabrication, The SiO_2/Si wafers were treated with OTS in the solution phase, as reported previously.[50] BPE-PTCDI NWs were drop-cast on the OTS-treated SiO_2/Si substrate. Gold electrodes (40 nm) were thermally evaporated using a shadow mask.

For the fabrication of the thin-film OPTs, BPE-PTCDI thin films (40 nm) were thermally evaporated onto OTS-treated SiO_2/Si substrates kept at 125 °C at a deposition rate of ≈0.1–0.2 Å s^{-1} under high vacuum (<5.0 × 10^{-6} Torr). Gold electrodes (40 nm) were thermally evaporated using a shadow mask to form top-contact thin-film OPTs. The current–voltage characteristics of the devices and the photoresponses upon on-and-off switching of light were measured in a N_2-filled glove box using a Keithley 4200-SCS semiconductor parametric analyzer.

Acknowledgements

This work was supported by a National Research Foundation of Korea (NRF) Grant funded by the Korean Government (MEST) (2011-0026424, 2011-0017174), and the Global Frontier Research Center for Advanced Soft Electronics (2011-0031628). H.Y. acknowledges financial support from the Global Ph.D. Fellowship funded by the National Research Foundation of Korea (NRF). Z.B. acknowledges financial support from the US Air Force Office of Scientific Research (FA9550-12-1-01906). The authors acknowledge Dr. Stefan Mannsfeld for helpful discussions on the TEM SAED patterns.

Received: July 5, 2012
Published online: September 7, 2012

[1] *Optoelectronic Sensors*, Vol. *1*, (Eds: D. Decoster, J. Harari), Wiley-ISTE, London **2009**.
[2] S. M. Sze, K. K. Ng, *Physics of Semiconductor Devices*, Vol. *3*, John Wiley & Sons, Hoboken, NJ USA **2007**.
[3] Y. L. Guo, C. Y. Du, G. Yu, C. A. Di, S. D. Jiang, H. X. Xi, J. Zheng, S. K. Yan, C. L. Yu, W. P. Hu, Y. Q. Liu, *Adv. Funct. Mater.* **2010**, *20*, 1019.
[4] H. Hwang, H. Kim, S. Nam, D. D. C. Bradley, C. S. Ha, Y. Kim, *Nanoscale* **2011**, *3*, 2275.
[5] H. Jiang, X. J. Yang, Z. D. Cui, Y. C. Liu, H. X. Li, W. P. Hu, *Appl. Phys. Lett.* **2009**, *94*, 123308.
[6] J. G. Labram, P. H. Wobkenberg, D. D. C. Bradley, T. D. Anthopoulos, *Org. Electron.* **2010**, *11*, 1250.
[7] Y. Y. Noh, D. Y. Kim, Y. Yoshida, K. Yase, B. J. Jung, E. Lim, H. K. Shim, *Appl. Phys. Lett.* **2005**, *86*, 043501.
[8] T. Pal, M. Arif, S. I. Khondaker, *Nanotechnology* **2010**, *21*, 325201.
[9] Q. X. Tang, L. Q. Li, Y. B. Song, Y. L. Liu, H. X. Li, W. Xu, Y. Q. Liu, W. P. Hu, D. B. Zhu, *Adv. Mater.* **2007**, *19*, 2624.
[10] Y. K. Che, H. L. Huang, M. A. Xu, C. Y. Zhang, B. R. Bunes, X. M. Yang, L. Zang, *J. Am. Chem. Soc.* **2011**, *133*, 1087.
[11] Q. Niu, Y. Zhou, L. Wang, J. Peng, J. Wang, J. Pei, Y. Cao, *Adv. Mater.* **2008**, *20*, 964.
[12] A. L. Briseno, S. C. B. Mannsfeld, S. A. Jenekhe, Z. Bao, Y. Xia, *Mater. Today* **2008**, *11*, 38.
[13] J. H. Oh, H. W. Lee, S. Mannsfeld, R. M. Stoltenberg, E. Jung, Y. W. Jin, J. M. Kim, J.-B. Yoo, Z. Bao, *Proc. Natl. Acad. Sci. USA* **2009**, *106*, 6065.
[14] L. Jiang, Y. Y. Fu, H. X. Li, W. P. Hu, *J. Am. Chem. Soc.* **2008**, *130*, 3937.
[15] Y. Che, X. Yang, S. Loser, L. Zang, *Nano Lett.* **2008**, *8*, 2219.
[16] H. Xin, F. S. Kim, S. A. Jenekhe, *J. Am. Chem. Soc.* **2008**, *130*, 5424.
[17] D. O'Carroll, I. Lieberwirth, G. Redmond, *Nat. Nanotechnol.* **2007**, *2*, 180.
[18] K. Takazawa, Y. Kitahama, Y. Kimura, G. Kido, *Nano Lett.* **2005**, *5*, 1293.
[19] K. Xiao, J. Tao, Z. Pan, A. A. Puretzky, I. N. Ivanov, S. J. Pennycook, D. B. Geohegan, *Angew. Chem. Int. Ed.* **2007**, *46*, 2650.
[20] C. Soci, A. Zhang, X.-Y. Bao, H. Kim, Y. Lo, D. Wang, *J. Nanosci. Nanotechnol.* **2010**, *10*, 1430.
[21] J. E. Park, B. Mukherjee, H. Cho, S. Kim, S. Pyo, *Synth. Met.* **2011**, *161*, 143.
[22] Y. Y. Noh, D. Y. Kim, K. Yase, *J. Appl. Phys.* **2005**, *98*, 074505.
[23] Y. L. Guo, C. A. Di, S. H. Ye, X. N. Sun, J. Zheng, Y. G. Wen, W. P. Wu, G. Yu, Y. Q. Liu, *Adv. Mater.* **2009**, *21*, 1954.
[24] S. Cho, J. Yuen, J. Y. Kim, K. Lee, A. J. Heeger, *Appl. Phys. Lett.* **2007**, *90*, 063511.
[25] K. H. Kim, S. Y. Bae, Y. S. Kim, J. A. Hur, M. H. Hoang, T. W. Lee, M. J. Cho, Y. Kim, M. Kim, J. I. Jin, S. J. Kim, K. Lee, S. J. Lee, D. H. Choi, *Adv. Mater.* **2011**, *23*, 3095.
[26] A. L. Briseno, S. C. B. Mannsfeld, X. M. Lu, Y. J. Xiong, S. A. Jenekhe, Z. N. Bao, Y. N. Xia, *Nano Lett.* **2007**, *7*, 668.
[27] G. Odian, *Principles of Polymerization*, Vol. *4*, Wiley-Interscience, Hoboken, NJ USA **2004**.
[28] J. Mizuguchi, *Acta Crystallogr., Sect. C: Cryst. Struct. Commun.* **1998**, *54*, 1479.
[29] V. C. Sundar, J. Zaumseil, V. Podzorov, E. Menard, R. L. Willett, T. Someya, M. E. Gershenson, J. A. Rogers, *Science* **2004**, *303*, 1644.
[30] V. Coropceanu, J. Cornil, D. A. da Silva, Y. Olivier, R. Silbey, J. L. Bredas, *Chem. Rev.* **2007**, *107*, 926.
[31] A. L. Briseno, S. C. B. Mannsfeld, C. Reese, J. M. Hancock, Y. Xiong, S. A. Jenekhe, Z. Bao, Y. Xia, *Nano Lett.* **2007**, *7*, 2847.
[32] K. Balakrishnan, A. Datar, R. Oitker, H. Chen, J. Zuo, L. Zang, *J. Am. Chem. Soc.* **2005**, *127*, 10496.
[33] M. M. Ling, P. Erk, M. Gomez, M. Könemann, J. Locklin, Z. N. Bao, *Adv. Mater.* **2007**, *19*, 1123.
[34] A. Liu, S. Zhao, S.-B. Rim, J. Wu, M. Könemann, P. Erk, P. Peumans, *Adv. Mater.* **2008**, *20*, 1065.
[35] J.-L. Bredas, D. Beljonne, V. Coropceanu, J. Cornil, *Chem. Rev.* **2004**, *104*, 4971.
[36] A. L. Briseno, S. C. B. Mannsfeld, S. A. Jenekhe, Z. Bao, Y. N. Xia, *Mater. Today* **2008**, *11*, 38.
[37] M. C. Hamilton, S. Martin, J. Kanicki, *IEEE Trans. Electron. Devices* **2004**, *51*, 877.
[38] X. H. Wang, K. Wasapinyokul, W. De Tan, R. Rawcliffe, A. J. Campbell, D. D. C. Bradley, *J. Appl. Phys.* **2010**, *107*, 024509.
[39] M. El Gemayel, M. Treier, C. Musumeci, C. Li, K. Müllen, P. Samori, *J. Am. Chem. Soc.* **2012**, *134*, 2429.
[40] A. J. Said, D. Recht, J. T. Sullivan, J. M. Warrender, T. Buonassisi, P. D. Persans, M. J. Aziz, *Appl. Phys. Lett.* **2011**, *99*, 073503.
[41] H.-W. Zan, W.-W. Tsai, H.-F. Meng, *Appl. Phys. Lett.* **2011**, *98*, 053305.
[42] L. A. A. Pettersson, L. S. Roman, O. Inganas, *J. Appl. Phys.* **2001**, *89*, 5564.
[43] M. Hiramoto, T. Imahigashi, M. Yokoyama, *Appl. Phys. Lett.* **1994**, *64*, 187.
[44] T. Katsume, M. Hiramoto, M. Yokoyama, *Appl. Phys. Lett.* **1996**, *69*, 3722.

[45] M. Hiramoto, A. Miki, M. Yoshida, M. Yokoyama, *Appl. Phys. Lett.* **2002**, *81*, 1500.
[46] J. Reynaert, V. I. Arkhipov, P. Heremans, J. Poortmans, *Adv. Funct. Mater.* **2006**, *16*, 784.
[47] A. L. Briseno, S. C. B. Mannsfeld, M. M. Ling, S. Liu, R. J. Tseng, C. Reese, M. E. Roberts, Y. Yang, F. Wudl, Z. Bao, *Nature* **2006**, *444*, 913.
[48] T. P. I. Saragi, R. Pudzich, T. Fuhrmann, J. Salbeck, *Appl. Phys. Lett.* **2004**, *84*, 2334.
[49] B. Mukherjee, M. Mukherjee, Y. Choi, S. Pyo, *ACS Appl. Mater. Interfaces* **2010**, *2*, 1614.
[50] Y. Ito, A. A. Virkar, S. Mannsfeld, J. H. Oh, M. Toney, J. Locklin, Z. Bao, *J. Am. Chem. Soc.* **2009**, *131*, 9396.